Control of the turbulent flow in a plane diffuser through optimized contoured cavities

A. Mariotti[a,*], G. Buresti[a], M.V. Salvetti[a]

[a] *Dipartimento di Ingegneria Civile e Industriale, Università di Pisa, Via G. Caruso 8, 56122 Pisa, Italia*

Abstract

A passive control strategy, which consists in introducing contoured cavities in solid walls, is applied to a plane asymmetric diffuser at a Reynolds number that implies fully-turbulent flow upstream of the diffuser divergent part. The analysed reference configuration, for which experimental and numerical data were available, is characterized by an area ratio of 4.7 and a divergence angle of 10 degrees. A large zone of steady flow separation is present in the diffuser without the introduction of the control. One and two subsequent contoured cavities are introduced in the divergent wall of the diffuser and a numerical optimization procedure is carried out to obtain the cavity geometry that maximizes the pressure recovery in the diffuser and minimizes the flow separation extent. The introduction of one optimized cavity leads to an increase in pressure recovery of the order of 6.7% and to a significant reduction of the separation extent, and further improvement (9.6%) is obtained by introducing two subsequent cavities in the divergent

*Corresponding author

Email addresses: alessandro.mariotti@for.unipi.it (A. Mariotti), g.buresti@ing.unipi.it (G. Buresti), mv.salvetti@ing.unipi.it (M.V. Salvetti)

wall. The most important geometrical parameters are also identified, and the robustness of the solution to small changes in their values and in the Reynolds number is assessed. The present results show that the proposed control strategy, previously tested in the laminar regime, is effective also for turbulent flows at higher Reynolds numbers. As already found for laminar flow, the success of the control is due both to a virtual geometry modification of the diffuser and to a favourable effect of the cavities in reducing the momentum losses near the wall.
Keywords: passive flow control, contoured cavities, flow separation, high Reynolds diffuser

---

1. Introduction

A crucial issue in many technological applications is the development of methodologies for flow control aimed at achieving desired design objectives (see e.g. [1–5]). In the present work, the interest lies in a further critical analysis of the performance of a passive method for the control of flow separation, previously tested in a diffuser configuration at low Reynolds numbers (laminar regime) [6].

The considered strategy is based on the introduction of appropriately-shaped cavities in the solid walls and was originally inspired by the combination of the ideas of trapped vortices and of multi-step afterbodies (see e.g. [7–9] and the references in [6]).

In particular, in [6] this passive control strategy was applied to the internal flow inside a plane symmetric diffuser at $Re = 500$, based on the inlet velocity on the axis and the half-width of the inlet section. The chosen

diffuser configuration, without the introduction of the control, was characterized by a large zone of steady asymmetrical boundary layer separation. A couple of symmetric contoured cavities was introduced in the diverging walls and an optimization of the cavity geometry was carried out to maximize the pressure recovery in the diffuser and to minimize the boundary layer separation extent. For the particular analysed configuration, the optimized-shape cavities permitted to achieve an increase in pressure recovery of the order of 13%. The optimal cavitities were found to have a depth that is definitely smaller than the thickness of the boundary layer and to contain a small recirculation region characterized by low velocity and where vorticity is reduced compared to the one present in the original configuration. Therefore, the proposed control method is significantly different from the one based on the trapped-vortex idea, which is characterized by large cavities containing an almost-constant vorticity bounded by a thin shear layer with a high vorticity value. In our strategy, the improvement of the diffuser efficiency and the reduction of the main flow separation were shown to derive from both a virtual geometry modification and a decrease of the loss of momentum in the near-wall region [6].

In the present work we focus on flow control in a diffuser configuration at higher Reynolds numbers, i.e. in the turbulent regime. Indeed, turbulent flows through geometric expansions are of interest for numerous engineering applications, such as the design of turbomachines, combustion engines , heat-exchangers, vehicles, power plants and wind tunnels (see e.g. [10–14]).

The test case used in this study is the turbulent flow in an asymmetric planar diffuser with a diverging angle of the inclined wall equal to 10

degrees and area ratio equal to 4.7. This diffuser configuration was investigated experimentally in [15–17]. In those experiments, the Reynolds number based on the width of the diffuser and on the centreline velocity at a reference section upstream of the divergent part of the diffuser, at which the flow was fully-developed turbulent, was 20000. Several numerical studies of the same flow configuration or of similar ones are also documented in the literature, e.g. [18–24]. More particularly, large-eddy simulations were carried out in [18, 19], while the RANS approach together with a number of different turbulence models was used in [20–24]. Therefore, the well consolidated experimental and numerical database available for this test-case permitted to carry out a detailed validation and calibration of the present numerical simulations, in which a RANS solver was used. Indeed, the first part of the present work concerns the comparison of the results obtained for the reference configuration (i.e. without cavities) with the experimental data in [15, 16] and with the numerical results in [18, 24]. The aim of this preliminary activity was the identification of a RANS turbulence model providing sufficiently accurate results with costs that could be acceptable for the subsequent numerical optimization of the diffuser with cavities.

The main goal of the present work is the assessment of the possible improvements of the diffuser efficiency that can be obtained through the control of flow separation by means of one or two appropriately-shaped cavities introduced in the diffuser divergent wall. In particular, an optimization procedure is carried out to find the optimal cavity shape and location, i.e. the ones producing the largest reduction in flow separation and, hence, the largest increase in diffuser efficiency. A complete optimization is carried out consid-

ering five different parameters characterizing the location and the geometry for each cavity. The main objective of the this activity is to compare the results obtained for the present application with the outcome of the previous investigation described in [6]. In particular, the comparison concerns the shape, location and dimensions of the optimal cavities, as well as the level of obtainable efficiency improvement. Moreover, a question at issue is whether the physical mechanisms leading to the success of the control strategy identified in [6] are still effective for the present diffuser configuration in the turbulent regime. The robustness of the control to small modifications of the optimum cavity parameters is also addressed and the effects of limited variations of the Reynolds number are also investigated.

Finally, the flow features and the performance of the configuration with two optimized contoured cavities are compared with those of a diffuser geometry obtained from a classical shape optimization of the diverging wall, based on Bézier curves.

2. Reference diffuser configuration

2.1. Geometry definition

The considered diffuser geometry is the same used for the simulations in [24] and is aimed at reproducing the experimental conditions in [15–17]. The tested diffuser can be divided into three sections: an inflow channel having constant width, an asymmetric diverging channel, and an outflow channel having again constant width (see Fig. 1). The inlet width, h is used here as reference length, while the outlet width is $k = 4.7h$. The diffuser area ratio, i.e. the ratio between the outlet and inlet cross-areas, is hence $AR = 4.7$. The

three diffuser parts have lengths equal to $l_1 = 65h$, $l_2 = 21h$ and $l_3 = 60h$ respectively, and they are connected through sharp edges. The upstream channel is sufficiently long to obtain a fully developed turbulent channel flow at the inlet of the diffuser diverging section, as in [24].

The adopted frame of reference is shown in Fig. 1. Note that in all the figures dimensionless coordinates are used, i.e. $X = x/h$ and $Y = y/h$ (capital letters are used for dimensionless parameters and lowercase letters for dimensional quantities).

2.2. Simulation set-up and numerical methodology

The simulations are carried out at $Re = hu/\nu = 20000$, where u is the x-velocity on the centreline at $X = -6.5$, which is chosen as the diffuser reference cross-section because therein the flow has already become fully-developed turbulent. This is witnessed by a velocity profile characterized by a ratio between the centreline velocity and the bulk velocity $u_{cl}/u_b = 1.14$ (see [25, 16]). This definition of the Reynolds number assures a matching with the experimental conditions in [15–17] and with the numerical ones in [18, 20, 22, 24]).

Two-dimensional simulations of the flow inside the diffuser were carried out by solving the Reynolds-Averaged Navier-Stokes equations using the commercial code Fluent, which is based on the finite-volume discretization method (see e.g. [26]). A preliminary unsteady simulation was carried out to check that a steady solution was obtained, as found in [18–24]. In this simulation, unsteady time advancing was chosen together with a second-order implicit scheme. The adopted dimensionless time step was $\Delta T = \Delta t/(l/u) = 9.75 \times 10^{-3}$, and represents the ratio between the dimen-

sional simulation advancing step Δt and the time necessary to a fluid particle moving at velocity u to pass through the diffuser length l. A second-order upwind scheme was used for the space discretization, together with a pressure-based algorithm to solve the momentum equations coupled with the continuity equation. The full-implicit coupling is achieved through an implicit discretization of the pressure gradient terms in the momentum equations and an implicit discretization of the face mass flux, including the Rhie-Chow pressure dissipation terms (see [26]).

Since after a numerical transient the flow inside the diffuser was found to become steady, in the following of the work only steady-state simulations were carried out. The above-described second-order upwind scheme and pressure-based coupled algorithm are used to solve also the steady-version of the Navier-Stokes equations.

As for the turbulence approach, three different models are used and compared, viz. the low Reynolds version of the standard κ-ω model (see [27]), the Shear-Stress Transport κ-ω (SST κ-ω) (see [28]), and the Reynolds Stress Model (RSM)(see [29]). For all the considered turbulence models, no wall functions are used and a suitable grid refinement is adopted in order to have $y^+ \leq 1$ at the wall.

As regards the boundary conditions, the velocity and the turbulence fields at the inlet of the diffuser (i.e. at $X = -65$) are specified by using uniform profiles, with velocity and turbulence intensity equal to 1 and 0.01, respectively. As previously mentioned, this condition assured that the upstream channel was sufficiently long to obtain a fully developed turbulent channel flow at the diffuser reference section ($X = -6.5$). A pressure boundary con-

dition is imposed at the outlet section ($X = 80$) and no-slip conditions are applied along the diffuser solid walls.

The computational grid is structured and is made of quadrilateral elements. Grid sensitivity analyses for all the three considered turbulence models have been carried out. For each turbulence model, four grids have been tested having 433×81, 997×300, 1994×600, and 3998×800 nodes, respectively. The coarsest grid is the same used in [24]. The finer ones are generated by reducing the dimension of the cells in the streamwise direction and their growth rate in the lateral direction. The same lateral dimension of the first cell near the wall is used for all grids to have the same value of the wall y^+.

2.3. Flow features and validation

Grid independence is checked on the mean pressure recovery coefficient $\overline{C_p}$, defined as follows:

$$\overline{C_p} = \frac{\overline{p_{out}} - \overline{p_{ref}}}{\frac{1}{2}\rho \overline{u_{ref}}^2}, \tag{1}$$

where $\overline{p_{ref}}$ and $\overline{u_{ref}}$ are the area-weighted average pressure and x-velocity (equal to the bulk velocity u_b) at the diffuser reference section $X = -6.5$, $\overline{p_{out}}$ is the area-weighted averaged pressure at the diffuser outlet ($X = 80$).

The mean pressure recovery is strictly related to the diffuser efficiency η, defined as:

$$\eta = \frac{\overline{C_p}}{\overline{C_{p_{ideal}}}}, \tag{2}$$

where the ideal pressure recovery coefficient $\overline{C_{p_{ideal}}}$ is calculated as:

$$\overline{C_{p_{ideal}}} = 1 - \left(\frac{1}{AR}\right)^2 = 1 - \left(\frac{h}{k}\right)^2. \tag{3}$$

Thus, for this diffuser (with area ratio $AR = 4.7$) we have $\overline{C_{p_{ideal}}} = 0.95$. We assumed that grid independence was reached when two different refined grids showed a difference of less than 1% in the mean pressure recovery coefficient. The main results of the grid sensitivity analyses are summarized in Table 1.

The SST κ-ω model shows grid independence already for the coarse mesh, i.e. 433×81. Conversely, the standard κ-ω model and the RSM reach grid independence only for the grid 1994×600, with a consequent increase of the required computational time for the simulation. Note that, at grid convergence, the predictions of $\overline{C_p}$ given by the different turbulence models differ by less than 2%. Based on this grid sensitivity analysis, the results for the SST κ-ω turbulence model on the grid 433×81 and the ones for the standard κ-ω and the Reynolds Stress Model on the grid 1994×600 are now described and compared against experimental and numerical available data [15, 16, 18].

The visualization of the flow streamlines in Fig. 2, obtained using the SST κ-ω turbulence model, shows that the diffuser is characterized by a large asymmetric zone of separated flow, which reattaches before the end of the diffuser.

The positions of the points in the separated region where the streamwise velocity is equal to zero are compared in Fig. 3 against the available experimental data by [15, 16] and those of the large-eddy simulation in [18]. The different turbulence models give similar predictions of the extent of the separated zone, which are in overall good agreement with the available experimental and numerical data. Note that at grid convergence the RSM does

not fail in the prediction of the separation process, as conversely observed in [24] on a grid having the same resolution as the coarsest one used in the present study.

The behaviour of the local pressure coefficient, C_p, along the diffuser walls is shown in Fig. 4. In agreement with [15, 16, 18], it is defined as:

$$C_p = \frac{p_{x,y} - \overline{p_{X=-1.69}}}{\frac{1}{2}\rho\overline{u_{X=-1.69}}^2} \tag{4}$$

where $p_{x,y}$ is the local pressure at the considered point and $\overline{p_{X=-1.69}}$ and $\overline{u_{X=-1.69}}$ are the area-weighted averaged velocity and pressure at section $X = -1.69$ [15, 16]. The κ-ω and the SST κ-ω models predict values for C_p on both walls that are slightly larger than the ones evaluated by using the RSM. Despite these discrepancies, the predictions given by all the considered turbulence models are inside the range of reference data.

We may thus conclude that the three different turbulence models give comparable results, in terms of pressure recovery and separation extent; moreover, they are in satisfactory agreement with the available experimental and numerical data. Since the SST κ-ω turbulence model reaches grid convergence for coarser grid resolution and, hence, it implies the lowest computational costs, the following simulations and the optimization of the configurations with cavities were carried out with the SST κ-ω turbulence model.

3. Diffuser with contoured cavities

The possible improvements of the diffuser efficiency that can be obtained by introducing a single contoured cavity in the diffuser divergent wall are first investigated. In particular, the optimized cavity shape that allows the

diffuser efficiency to be maximized in the same operating conditions of Sec. 2.2 is described in Sec. 3.2 and the robustness of the results is addressed in Sec. 3.3. The same optimization procedure used for the single cavity is then applied to maximize the efficiency of a diffuser with two subsequent cavities (see Sec. 3.4). Finally, the robustness of the optimized cavity configuration to moderate changes in the Reynolds number is investigated in Sec. 3.5.

3.1. Optimization procedure

The optimization procedure is the following: in each optimization loop, the diffuser geometry is defined, the computational grid is generated and the cost function is evaluated through the numerical simulation of the flow inside the diffuser. The optimization algorithm determines the modified configurations and the loop is repeated until a convergence criterion is reached and the final optimized geometry is obtained. The optimization algorithm is the same as in [6], i.e. the Multi-Objective Genetic Algorithm MOGA-II (see e.g. [30, 31]), used with a single-objective function (see e.g. [32] for the use of MOGA-II in single-objective optimization). In all cases, the parameter space is discretized in intervals of uniform size; an initial population is generated through a pseudo-random Sobol sequence [31], by using a subset of the specified discrete parameter values. The population evolves through the following reproduction operators: directional crossover, mutation and selection [31]. The probability of directional crossover, of mutation and of selection, are set to 0.5, 0.1 and 0.05.

As already done in [6], the parameter $\overline{C_p}$ is chosen as the objective function. Nonetheless, after the optimization the total dissipation inside the diffuser is also evaluated through the Bobyleff-Forsyth formula (see e.g. [33, 34])

in order to have a further confirmation of the results.

3.2. Optimization of a single contoured cavity

One single cavity is positioned in the diverging wall of the diffuser. The cavity starts with a sharp edge, has an upstream part with a semi-elliptical shape, and ends with a spline up to a point that can be along the original diffuser diverging wall or inside the diffuser. The final point of the cavity is then connected to the end of the diffuser diverging part through a straight line. The spline and the straight line are tangent (see Fig. 5). Compared to the optimizations carried out in [6], this cavity shape can end with a *bulge* inside the original diffuser profile, which is expected to promote the flow reattachment after the recirculation inside the cavity. Indeed, this reattachment has been found in [6] to be essential for an efficient control of the subsequent main separation.

An optimization of the cavity shape is then carried out in order to maximize $\overline{C_p}$ and, hence, the efficiency η of the diffuser. The optimization parameters are: the distance from the beginning of the diffuser diverging part to the upstream edge of the cavity, s/h, the cavity total length, t/h, the ellipse axis parallel to the original diffuser diverging wall, a/h, the ellipse axis normal to the diffuser diverging wall, b/h, and the normal distance from the end point of the cavity to the original diverging wall (i.e. the *bulge* extent), r/h (see Fig. 5).

The upstream edge of the cavity and its ending point are allowed to vary along the whole diffuser diverging wall, whereas, based on the results obtained in [6], the chosen range of variation of the cavity axes, a and b, are respectively chosen to be $0.02h - 0.6h$ and $0.01h - 0.4h$. The normal distance

from the end point of the cavity to the original diverging wall, r/h, is allowed to vary from 0 (i.e. with the spline tangent to the diffuser divergent wall) to $2h$. The parameter space was discretized by using uniform intervals having a width of 0.02, 0.01, 0.2, 0.2, and 0.025 for a/h, b/h, s/h, t/h, and r/h respectively. These discrete parameter values are explored by the MOGA-II algorithm.

The initial population is composed of 25 individuals, distributed in the discretized parameter space by means of the previously cited Sobol sequence. Then, 7 additional generations were created by the optimization algorithm, each one composed of 25 individuals. Starting from the sixth generation, most of the new individuals created by the algorithm are characterized by $s/h = 4.2 - 5.4$, $a/h = 0.18 - 0.40$, $b/h = 0.11 - 0.13$, $t/h = 10.6 - 11.4$ and $r/h = 0.95 - 1$ (8 over 25 individuals in the seventh generation). All these configurations give values of the objective function which differ from the maximum one by less than 0.1%. Moreover, no further improvement of the maximum value of the objective function is found between the sixth and the seventh generations.

From the visualization of the streamlines in the diffuser with one optimized cavity in Fig. 6, it is evident that the flow separates at the cavity edge but reattaches immediately downstream, forming a small recirculation region; furthermore, the subsequent flow separation is delayed and its extent is reduced (compare with Fig. 2).

The detailed comparison between the diffuser without cavities and the diffuser with one optimized cavity in terms of mean pressure coefficient at different sections ($\overline{C_{p_x}}$, defined as in Eq. (1), by using the area-weighted av-

erage pressure at the local section) and of separated region extent are shown in Fig. 7(a) and in Fig. 7(b), respectively. The starting point of the main separation zone moves from $X_{sep} = 3.8$ to $X_{sep} = 15.1$ and the reattachment point from $X_{reatt} = 28.8$ to $X_{reatt} = 30.5$. This in turn implies a reduction of the pressure losses in the diffuser divergent part. A pressure recovery increase of 6.9% is found compared to the sharp-edged diffuser without cavity ($\overline{C_p}$ increases from 0.716 to 0.765 in the configuration with optimum cavities). The total dissipation Φ_t inside the diffuser also confirms the improvement of the diffuser performance. A reduction of the dissipation of 3.7% is indeed found.

An unsteady simulation of the flow inside the diffuser with optimized cavities was also carried out, to check that the flow is steady even after the introduction of the contoured cavity in the diffuser diverging wall. A steady solution was reached, which coincides with the one of the steady-state simulation.

Regarding the optimum cavity parameters, the semi-ellipse axis normal to the diffuser diverging wall b/h is important because it determines the width of the first recirculation region. Its optimum value is found to be $b/h = 0.11 - 0.13$, and thus it is small compared with the width of the fully-developed turbulent channel flow. On the other hand, the ellipse axis a/h is again found to have a negligible effect as in [6].

Fundamental parameters are also t/h and r/h, which determine together the position and the width of the *bulge*, i.e. where and how much the diffuser is locally narrowed. Large values of t/h have the effect of delaying the flow separation. On the other hand, to be effective the *bulge* has to be deep enough to allow the streamlines to reattach after the cavity but, in turn, this creates a

local narrowing of the diffuser, which causes a local reduction of the pressure recovery. Therefore, the optimum configuration is a compromise between the total length of the cavity, t/h, and the value of the normal distance from the end point of the cavity to the original diverging wall, r/h (see Sec. 3.3). In this case, the ranges of the optimum values are $t/h = 10.6 - 11.4$ and $r/h = 0.975 - 1$, and they cause a significant change in the shape of the downstream part of the diffuser (see Fig. 7(b)).

The optimum value of the cavity starting point is $s/h = 4.2 - 5.4$, which roughly corresponds to the beginning of the separated region in the reference diffuser configuration. Conversely, in [6] all the optimum cavities started at the beginning of the diffuser divergent part and the possible reasons for this difference will be discussed in Sec. 3.3.

As was done in [6], the main mechanisms through which the boundary layer separation is delayed and the pressure recovery performance of the diffuser is improved were investigated. First of all, it is evident from Fig. 6 that, as already observed in [6], the optimized configuration is characterized by the presence of a small closed recirculation region. This region, characterized by very low velocity values, does not correspond to a local concentration of vorticity, but rather to a zone where vorticity is reduced compared to the one present in the original configuration. The situation is then perfectly analogous to the one shown in Fig. 9 of [6]. The streamlines of the outer flow close to the boundary of the recirculation zone are also modified by the presence of the cavity. In order to investigate on the influence of the virtual geometry modification of the diffuser lateral surface caused by the geometry of the streamlines outside the cavity recirculation region, a simulation was

then carried out with a diffuser in which the streamline bounding this recirculation region was replaced by a solid surface. This gives a diffuser with a modified geometry compared to the original one; this new geometry is an additional output of the cavity optimization procedure.

The modified diffuser without cavities does indeed produce a significant performance improvement over the original reference configuration, giving a $\overline{C_p}$ value of 0.758, i.e. a 5.9% increase over the reference value, compared to the 6.9% gain for the diffuser with optimized cavities. Correspondingly, a reduction in dissipation of 3.1% is found, and should be compared to the value of 3.7% for the diffuser with optimized cavities. The results obtained for the modified diffuser are compared in more detail to those of the reference configuration and of the diffuser with optimized cavities in Figs. 7(a) and 7(c), where the variations of $\overline{C_{p_x}}$ along the three diffusers are shown together with the corresponding extents of the separation regions. As can be seen, compared to the reference configuration, there is an analogous increase in pressure at the beginning of the diffuser diverging part for both the modified diffuser and the one with the optimized cavities, due to the local geometry modification. More downstream, the pressure losses are lower than in the reference configuration due to a reduction of the separated region extent. This latter effect is clearly more pronounced for the diffuser with cavities, which is the case characterized by the smallest separated flow region. As already discussed in detail in [6], the specific physical mechanism responsible for the positive effect of the cavities on flow separation is the reduction of momentum losses near the wall due to the relaxation of the no-slip condition.

3.3. Robustness analysis of the optimized flow control device

In this section the effects of some deviations of the cavity geometrical parameters from the optimal ones are investigated, in order to ascertain whether this flow control device is robust with respect to small variations of the cavity geometry and position.

First of all, we focus on the ellipse axis normal to the diffuser diverging wall b/h. The robustness to variations of b/h is analysed by varying this parameter in the range $0.03 - 0.2$; conversely, the other cavity parameters are kept fixed to their optimum values, i.e. $s/h = 4.2-5.4$, $t/h = 10.6-11.4$, and $r/h = 0.95-1$. Considering the small influence of the cavity axis parallel to the wall, a fixed value was chosen, viz. $a/b = 2$.

The proposed configuration is robust in the whole considered range of values of b/h. Indeed, the pattern of the streamlines is similar to the one of the optimum configuration and the performance of the diffuser with cavities is always better than the one of the diffuser without cavities. In particular, compared to the reference diffuser the efficiency gains are always equal or above 6% (see Fig. 8).

The parameter b/h determines the depth of the recirculation region produced by the cavity, whose extension increases with increasing values of b/h. At the same time, the presence of a *bulge* improves the possibility of having a flow reattachment after the cavity, even for high values of b/h. Thus, also for cavities that are higher than the optimum ones the flow reattaches immediately downstream of the recirculation region produced by the cavity. Note that this does not happen for the cavities without the *bulge* previously proposed in [6], where the optimum value of the parameter b/h is strictly

related to the flow reattachment downstream of the recirculation region produced by the cavity and the diffuser efficiency may become even worse than the one of the diffuser without cavities for excessive values of b/h.

As can be expected, the effect of momentum loss reduction near the wall is stronger for deeper cavities. Indeed, for values of b/h above the optimum, the extent of the main separation region is further reduced compared to the one corresponding to the optimum values of the parameters. On the other hand, in these cases the recirculation region in the cavity is wider and produces a local narrowing of the diffuser cross section which, in turn, implies local decreases in the pressure recovery. Conversely, for values of b/h below the optimum one, the recirculation region in the cavity is smaller: this implies a lower local narrowing of the diffuser cross-section but also produces a lower reduction of the main separation region. Thus, the best compromise between the two effects has been identified by the optimization algorithm but, at the same time, this analysis highlights that this flow control device is very robust to small variations of b/h around the optimum ones and that the introduction of the *bulge* increases the robustness of the device to the parameter b/h compared to the cavity geometry without *bulge* proposed in [6].

The robustness of the flow-control device to the position and the magnitude of the *bulge* is investigated by identifying the simultaneous effect of the variation of t/h and r/h. The parameter t/h is varied in the range $4 - 14$, while r/h is varied in the range $0.6 - 1.2$. The parameter space is discretized by using a uniform interval of size equal to 2 for t/h and 0.1 for r/h, i.e. 6×7 discrete parameter values, corresponding to 42 positions of the

bulge, are analysed. The other cavity parameters are kept fixed at $s/h = 5$, $b/h = 0.12$ and $a/b = 2$. The response surface for the diffuser efficiency to the parameters t/h and r/h is shown in Fig. 9. A multivariate polynomial interpolation based on the Singular Value Decomposition algorithm, with a second order polynomial, was used to build this response surface (see e.g. [31]). Figure 9 confirms that for longer cavities larger *bulges* are required to achieve the reattachment of the flow downstream of the separated region inside the cavity and to maximize the diffuser efficiency. Conversely, for shorter cavities small *bulges* are needed. Moreover, the device is robust for small variation of the *bulge* shape compared to the optimized one.

Finally, the effect of the parameter s/h is analysed. The cavity starting point is moved upstream of its optimum value by keeping the rear geometry of the diffuser coincident with the optimum one, i.e. s/h is varied while $s/h + t/h$ is kept fixed to avoid a change of the relative position and of the magnitude of the *bulge*. On the other hand, no analysis is carried out with the starting point of the cavity placed downstream of the optimum one, i.e. for values of s/h above the optimum, because in those cases the cavities would have been placed in a region where the main flow separation has already occurred. Thus, in this analysis the parameter s/h is varied in the range $0-5$. The other cavity parameters are kept fixed to $s/h+t/h = 16$, $r/h = 1$, $b/h = 0.12$ and $a/b = 2$.

The performance of the diffuser always decreases by moving the cavity starting point upstream of its optimum position (see Fig. 10). For values of $1 < s/h < 5$ the performance of the diffuser with the cavity remains better than the one of the diffuser without the cavity, while for $0 < s/h < 1$ the

efficiency of the diffuser with cavity is lower compared to the reference one.

The optimum position of the cavity starting point and the result of the robustness to s/h variations represent the main differences between the characteristics of the optimum cavities for the present diffuser configuration and the one analysed in [6]. In the present case the optimum value of the cavity starting point roughly corresponds to the beginning of the separated region in the reference diffuser configuration, while, as previously pointed out, a cavity placed at the beginning of the diffuser divergent part causes an abrupt decrease of the flow control device performance. Conversely, in [6] all the optimum cavities started at the beginning of the diffuser divergent part.

In order to analyse the possible reasons for this difference, the streamlines inside two cavities that start at the beginning of the diffuser divergent part for both the diffuser considered in [6] and the present one are shown in Figs. 11(a) and 11(c), respectively. Moreover, a comparison between the recirculation region extents in the two flow regimes are presented in Figs. 11(b) and 11(d). The walls of the corresponding reference diffuser configurations are also shown by means of dashed lines.

In both cases the cavity causes an immediate separation of the boundary layer, which reattaches downstream of the recirculation region inside the cavity. For the diffuser in [6] the streamline bounding the recirculation region is always outside the diverging wall of the corresponding reference diffuser configuration (see Fig. 11(b)) and locally produces a wider diffuser cross-section, which leads to an improvement of the local mean pressure recovery coefficient. Conversely, in the present case the streamline bounding the recirculation region is inside the diverging wall of the corresponding reference

diffuser (see Fig. 11(d)). Thus, the recirculation region inside the cavity produces a local narrowing of the cross-section and this locally reduces the value of $\overline{C_p}$. For this reason in the present configuration it is not convenient to place the cavity upstream of the location at which the flow would separate anyway.

3.4. Optimization of two subsequent contoured cavities

In this section two subsequent cavities are considered in order to investigate whether a second cavity could further improve the diffuser efficiency and reduce the flow separation. The two cavities are introduced in the diverging wall of the diffuser. Both cavities start with a sharp edge, have an upstream part with a semi-elliptical shape, and end with a spline up to a point that can be along the original diverging wall of the diffuser or inside it. The starting point of the second cavity coincides with the ending point of the spline of the first cavity. The ending point of the second cavity is then connected to the end of the diffuser diverging part through a straight line, which is tangent to the preceding spline (see Fig. 12).

The same optimization carried out for the single cavity (see Sec. 3.1) was used to identify the shape of the device that maximizes the diffuser efficiency. The optimization parameters are: the distance from the beginning of the diffuser diverging part to the upstream edge of the first cavity, s/h, the first and second cavity total lengths, t_1/h and t_2/h, the ellipse axes normal to the diffuser diverging wall of the two cavities, b_1/h and b_2/h, and the normal distances from the end points of the cavities to the original diverging wall, r_1/h and r_2/h (see Fig. 12). Again, since the ellipse axes parallel to the diffuser diverging wall have practically no importance (see Sec. 3.2), the

upstream parts of the cavities have a 2:1 semi-elliptical shape (the ellipse axis parallel to the diffuser diverging wall is equal to twice the ellipse axis normal to the diffuser diverging wall).

The start and end points of both cavities (s_1/h, t_1/h and t_2/h) are allowed to vary along the whole diffuser diverging wall, while the considered ranges for the axes b_1/h and b_2/h are from $0.01h$ to $0.2h$. The normal distances from the end points of the cavities to the original diverging wall r_1/h and r_2/h are allowed to vary from 0 to $1.5h$ and to $2.5h$ respectively.

The parameter space is discretized by using uniform intervals having a width of 0.01 for b_1/h and b_2/h, 0.2 for s/h, t_1/h and t_2/h, 0.025 for r_1/h and r_2/h. These discrete parameter values are explored by the MOGA-II algorithm. The initial population was composed of 50 individuals, distributed in the discretized parameter space by means of the previously cited Sobol sequence. Then, 11 additional generations were created by the optimization algorithm, each one composed of 50 individuals. Starting from the tenth generation, most of the new individuals created by the algorithm are characterized by $s/h = 4.8{-}5.2$, $b_1/h = 0.04{-}0.07$, $b_2/h = 0.04{-}0.06$, $t_1/h = 5.4{-}6.0$, $t_2/h = 8.6 - 9.2$, $r_1/h = 0.825 - 0.875$ and $r_2/h = 0.726 - 0.850$ (11 over 50 individuals in the eleventh generation), which correspond to the highest values of the objective function. Moreover, the maximum values of the objective function reached in the tenth and eleventh generation differ by less than 0.2%.

Suitably-shaped double cavities lead to a successful control of flow separation. From the visualization of the streamlines in the diffuser with double optimized cavities, sketched in Fig. 13, it is evident that the flow separates at

the upstream edges of the cavities and reattaches immediately downstream, forming two small recirculation regions; the subsequent main flow separation is delayed and its extent is reduced. Also in this case, an additional unsteady simulation of the flow inside the diffuser with optimized cavities was carried out and confirmed that the flow is steady even after the introduction of the contoured cavities and that the results of the steady and unsteady simulations coincide.

The detailed comparisons between the diffuser without cavities and the diffuser with two optimized cavities in terms of mean pressure coefficient and separated region extents are shown in Fig. 14(a) and in Fig. 14(b), respectively. The starting point of the separation bubble is further moved downstream ($X_{sep} = 17.3$ and $X_{reatt} = 31.2$). This produces a decrease of the pressure losses in the diffuser divergent part, together with a further reduction of the separated region extent. A pressure recovery increase of 9.6% is found compared to the sharp-edged diffuser without cavity ($\overline{C_p}$ increases from 0.716 to 0.785 in the configuration with optimum cavities). The total dissipation Φ_t inside the diffuser also confirms the optimization results. A reduction of the dissipation of 6.5% is indeed found. As for the optimum cavity parameters, the optimum values of the semi-ellipse axes normal to the diffuser diverging walls, b_1/h and b_2/h, are smaller compared to the optimum value for the single cavity. Great importance have also the couples of parameters t_1/h, r_1/h and t_2/h, r_2/h, which determine the position and the magnitude of the two *bulges* that allow the streamlines to reattach after the recirculation in the cavities and to move the main separation downstream. As already highlighted for a single cavity in Sec. 3.3, since the *bulges* cause a

local reduction of the diffuser cross-section and, thus, of the pressure recovery in the diffuser (see Fig. 14(a)), an optimum compromise exists between the total lengths of the cavities and the magnitudes of the *bulges*. The optimum value of the first cavity starting point is again at the beginning of the separated region in the reference diffuser.

Also for the diffuser with double cavities the outer streamlines adjacent to the boundary of the recirculation zones are modified by the presence of the cavities and of two *bulges* (see Fig. 13). As had been done for the diffuser with a single cavity, a simulation was carried out for a diffuser in which the streamline bounding the two recirculation regions of the optimized cavities was replaced by a solid surface, in order to investigate on the impact of the diffuser virtual shaping produced by the cavities.

The modified diffuser without cavities gives a significant improvement over the original reference configuration but it does not reach the values of the diffuser with optimized cavities. The resulting value of $\overline{C_p}$ is indeed 0.774, with a 8.1% increase over the reference value, compared to the 9.6% gain for the diffuser with optimized cavities. Correspondingly, a reduction in dissipation of 4.7% is found, and should be compared to the value of 6.5% for the diffuser with optimized cavities. The results obtained for the modified diffuser are compared in more detail with those of the reference configuration and of the diffuser with optimized cavities in Figs. 14(a) and 14(c).

3.5. Effect of Reynolds number

In this section the effect of the modification of the Reynolds number of the flow upstream of the diffuser is investigated. To this aim, the performance of the diffusers with one and two subsequent cavities, whose geometries were

optimized at $Re = 20000$, is analysed at $Re = 10000, 15000, 25000, 30000$ and is compared to the one of the reference diffuser at the same Reynolds numbers. This can be considered as a further analysis of the robustness of the control device, which is tested in off-design conditions obtained by modifying the flow Reynolds number. As regards the reference diffuser configuration, also for the new values of the Reynolds number all the velocity profiles at the section $X = -6.5$ are fully developed turbulent and analogous flow patterns are found, with only slight modifications of $\overline{C_p}$ (as also found in [23]): $\overline{C_p} = 0.702, 0.712, 0.725, 0.731$, respectively for $Re = 10000, 15000, 25000, 30000$.

Although the devices have not been optimized for these Reynolds numbers, they lead to effective increases in the diffuser efficiency compared to the one of the reference diffuser configuration in the same operating conditions. In particular the gains obtained by the introduction of one contoured cavity are 5.4%, 6.1%, 6.5%, 6.4% for $Re = 10000, 15000, 25000, 30000$, respectively. Two subsequent cavities lead to an increase of 7.8%, 8.8%, 9.2% and 9.0% for the same Reynolds numbers. The evaluation of the total dissipation inside the diffusers confirmed the above results.

4. Classical shape optimization of the diffuser geometry

In this Section, the results of a classical shape optimization of the diffuser divergent wall, obtained by using Bézier curves, are described and compared with the ones of the diffuser with two contoured cavities.

In particular, the diffuser divergent wall is defined by using eight Bézier control points. The first and the last control points have been kept fixed at the beginning and at the end of the divergent part of the diffuser, i.e. A=

$[0, h]$ and A'$= [21h, 4.7h]$. The coordinates of the six remaining control points represent the parameters to be optimized, thus the Bézier curve giving the diffuser divergent wall is defined by 12 degrees of freedom. The x-coordinate of these points can vary in the range $0 - 21h$, and the y-coordinate from $-4.5h$ to $6.5h$. These ranges are discretized by using 20 intervals for the x-coordinate and 60 intervals for the y-coordinate, both uniformly distributed. The automatic procedure used for the classical wall-shape optimization is the same as in Sec. 3.1.

The resulting optimized diffuser geometry is compared with the diffuser with two optimized cavities in Fig. 15(b), where the extent of separations are also shown. The diffuser with optimized Bézier curve does not present the formation of localized recirculation regions along the diffuser divergent part. But the most striking difference between the two configurations is in the last part of the divergent wall. Indeed, the wall geometry optimized through the Bézier curve gives rise to a steeper widening of the cross-section at the end of the diffuser divergent part and this allows the main recirculation region to be further moved downstream and slightly reduced compared to the configuration with two cavities. As can be seen from the comparison of the $\overline{C_{p_x}}$ (Fig. 15(a)), in the first part of the diffuser divergent wall, where cavities are presents, the pressure recovery is larger for the diffuser with optimized cavities, while in the second part the diffuser with optimized Bézier curve has a better performance due to the previously highlighted differences in the separation zone. As a result the diffuser with the optimized Bézier curve produces a total increase of the pressure recovery coefficient that is equal to the one obtained with two optimized contour cavities (9.6% compared to

the reference configuration). Note that the shape of the rear part of the diffuser divergent wall given by Bézier optimization could not be obtained with the optimized cavities because of a geometrical constraint introduced in order to reduce the number of degrees of freedom. Indeed, the final point of the second cavity is forced to be connected to the end of the diffuser diverging part through a straight line (see Fig. 5). However, it may be inferred from the analysis of $\overline{C_{p_x}}$ that the performance of the diffuser might be further enhanced by combining the optimized cavities with the rear part of the Bézier optimized wall.

To check the validity of this assumption, the rear part of the diffuser with cavities is replaced by the rear part of the optimized Bézier curve, as shown in Fig. 16(b). This diffuser configuration produces an increase of the pressure recovery of 10.5% ($\overline{C_p} = 0.791$). As can be seen in Fig. 16(a), the pressure recovery in the modified geometry of the rear part of the divergent wall is beneficial also for the diffuser with cavities, allowing the recirculation region to be moved more downstream. On the other hand, thanks to the reduction of momentum losses in the recirculations produced by the cavities, the separation is also further reduced compared to the one given by the Bézier optimization (see Fig. 16(b)). Note that the last configuration could probably have been obtained by an optimization of the case with two cavities in which the previously mentioned constraint is released. However, this has not been done herein, since it would involve a large number of degrees of freedom and thus a significant computational effort without adding much to the present analysis.

Note that both the considered strategies, optimized cavities and classical

shape optimization, produce a significantly larger gain in pressure recovery than the one obtained in [35] by optimizing the same diffuser in order to have an incipient flow separation along the diffuser divergent part [36] (the increase in pressure recovery in [35] is about 3.3%). From the analysis of the skin friction coefficient along the diffuser diverging wall (see Fig. 17), it is clear that the present optimized configurations are characterized by wall shear stresses that are significantly different from zero. In particular, considering the configuration with two cavities, it may be noted that zones of negative friction, corresponding to the recirculation regions, alternate with positive friction values in the subsequent wall portions where the boundary layer reattaches.

5. Conclusions

The goal of the present study was to further assess the potential of a strategy for passive flow control based on the introduction of optimized-shape cavities in the solid walls, whose good performance had previously been assessed in the laminar regime for a plane symmetric diffuser with a total divergence angle of 7 degrees and an area ratio of 2 (see [6]). In particular, the turbulent flow in an asymmetric diffuser with a divergence angle of 10 degrees and an area ratio of 4.7 was considered. This different and more challenging configuration was chosen because experimental and numerical results were available at a reference Reynolds number of $Re = 20000$ (corresponding to turbulent conditions), which could be exploited for the validation of the RANS solver that had to be used to allow an affordable numerical optimization to be carried out.

One or two subsequent contoured cavities were introduced in the diffuser divergent wall and optimizations were carried out in order to identify the cavity geometries and locations allowing the pressure recovery, and thus the diffuser efficiency, to be maximized. Each cavity geometry was defined by using five parameters, namely the cavity starting point, the two ellipse axes, its total length, and the value of the final *bulge* of the cavity, i.e. of the distance from the end of the cavity to the original diffuser diverging wall. Note that the possibility of allowing the presence of this *bulge* after each cavity had not been considered in the laminar case in [6], but it has been included here since it was thought that it could promote the flow reattachment after the recirculation inside the cavities and thus delay the downstream main separation. The use of optimized contoured cavities leads to significant reductions of the flow separation in the diffuser, and to increases in efficiency of the order of 6.9% and 9.6% compared to the original configuration, for one and two cavities respectively. The improvement in the diffuser performance is also confirmed by the reduction of the total dissipation inside the diffuser (-3.7% and -6.5%).

The flow topology in the optimized diffuser configurations is analogous to the one observed in [6]: the flow separates at the upstream sharp edge of each cavity and rapidly reattaches, forming closed recirculation regions, characterized by low values of velocity and vorticity, within and immediately downstream of the cavities. Furthermore, the subsequent flow separation is delayed and its extent is reduced.

The mechanisms leading to the success of the control strategy have been found to be the same already discussed in some detail in [6]. In particu-

lar, there is a combination of two effects: (i) a virtual modification of the diffuser geometry "seen" by the flow outside the recirculation region of the cavities and (ii) the local effect of the cavity recirculation region itself, which reduces the momentum losses near the wall. In order to separate these two mechanisms, simulations were also performed of the flow inside a modified diffuser with solid lateral walls coinciding with the streamlines bounding the recirculation regions produced by the optimized cavities. The results of the comparison between the various configurations show that both the new "virtual geometry" of the diffuser and the reduced losses in the near-wall region give a significant contribution to the good performance of the diffuser with cavities. However, in the present case the contribution of the virtual shape modification is noticeably larger than in [6]; this is probably due to the fact that the *bulge*, which was not considered in the laminar case, strongly modifies the diffuser shape and this gives a large contribution to the efficiency improvement.

The optimized cavities are similar to the optimal ones for the configuration in [6]. In particular, they are characterized by a small dimension normal to the diverging wall, b, compared to the diffuser width h; this has the consequence that the region inside the contoured cavities does not correspond to a local concentration of vorticity, but rather to a zone where vorticity is reduced compared to the one that is present in the original configuration. As was already observed for the configuration analysed in [6], this suggests that the present control device is more closely related to the multi-step afterbody concept than to the production of large trapped vortices. The main difference with the findings in [6] is that in the present configuration the optimum

value of the cavity starting point, s/h, almost corresponds to the beginning of the separated region in the reference diffuser configuration. Conversely, in [6] the optimized cavity was placed at the beginning of the diffuser divergent part. This difference can be explained by the fact that in that configuration the streamline bounding the recirculation region was always outside the diverging wall of the corresponding reference diffuser configuration, while in the present case the same streamline is inside the diverging wall of the corresponding reference diffuser. Thus, the recirculation region inside the cavity produces a local narrowing of the cross-section and this locally reduces the value of $\overline{C_p}$. Hence, it is convenient to place the cavities only where the flow would separate anyway. Moreover, the couple of parameters t/h and r/h determine together the position and the magnitude of the *bulge* and an optimum compromise exists between the values of these parameters. Indeed, to be effective the *bulge* has to be large enough to allow the streamlines to reattach after the cavity but, in turn, this creates a local narrowing of the diffuser, which causes a local reduction of the pressure recovery.

The device is generally robust to small variations of the different parameters. In particular, the sensitivity to b is further reduced compared to what observed in [6], probably because the presence of the *bulge* facilitates the flow reattachment after the cavity. Finally, the performance of the diffuser with one and two subsequent cavities, optimized at $Re = 20000$, was shown to be more than satisfactory also at different Reynolds numbers, namely $Re = 10000, 15000, 25000, 30000$. Indeed, significant increases were found in the diffuser efficiency compared to the one of the reference configuration in the same operating conditions; therefore, the introduction of the optimized-

contour cavities can be considered robust also to small changes in Reynolds number.

Finally, a classical shape optimization of the diffuser divergent wall was carried out by using a Bézier curve with 12 degrees of freedom. The resulting configuration was found to give the same gain in pressure recovery previously obtained with two cavities. However, it appears that in the first part of the wall the cavities give a larger pressure recovery than the optimal wall shape, whereas this latter configuration outperforms the one with cavities in the last part of the divergent wall thanks to a steeper widening of the cross-section which, in turn, allows the main recirculation to be reduced and moved further downstream. The same shape of the last part of the divergent wall could not be obtained in the case of the cavities, due to a geometrical constraint introduced to limit the number of degrees of freedom involved in the optimization process. Based on these observations, an additional simulation was carried out in which the optimal cavities are combined to the shape of the last part of the divergent wall given by Bézier optimization. This last configuration leads to a pressure recovery gain of 10.5%, i.e. larger than both the previously considered solutions; this confirms the beneficial effect of the introduction of the contoured cavities, even for an already "optimized" geometry.

Acknowledgments

The authors wish to thank Elisabetta Baroni for her precious contribution in carrying out the numerical simulations.

References

[1] J. C. Lin, Review of research on low-profile vortex generators to control boundary-layer separation, Prog. Aerosp. Sci. 38 (4-5) (2002) 389–420.

[2] S. S. Collis, R. D. Joslin, A. Seifert, V. Theofilis, Issues in active flow control: Theory, control, simulation, and experiment, Prog. Aerosp. Sci. 40(4-5) (2004) 237–289.

[3] P. R. Ashill, J. L. Fulker, K. C. Hackett, A review of recent developments in flow control, Aeronaut. J. 109 (2005) 205–232.

[4] M. Gad-el-Hak, Flow control: Passive, active, and reactive flow management, Cambridge University Press, London, United Kingdom. (2007).

[5] H. Choi, W. P. Jeon, J. Kim, Control of flow over a bluff body, Annu. Rev. Fluid Mech. 40 (2008) 113–139.

[6] A. Mariotti, A. N. Grozescu, G. Buresti, M. V. Salvetti, Separation control and efficiency improvement in a 2D diffuser by means of contoured cavities, Eur. J. Mech. B-Fluid 41 (2013) 138–149.

[7] F. Ringleb, Separation control by trapped vortices, in: Lachmann, G.V. (Ed.), Boundary layer and flow control, Vol. 1, Pergamon Press, Oxford (1961) 265–294.

[8] J. A. C. Kentfield, Short, multi-step, afterbody fairings, J. Aircraft 21 (5) (1984) 351–352.

[9] A. Iollo, L. Zannetti, Trapped vortex optimal control by suction and blowing at the wall, Eur. J. Mech. B-Fluid 20 (2001) 7–24.

[10] A. Klein, Characteristic of combustor diffusers, Prog. Aerosp. Sci. 31 (1995) 171–271.

[11] E. Göttlich, Research on the aerodynamics of intermediate turbine diffusers, Prog. Aerosp. Sci. 47 (2011) 249–279.

[12] H. Lan, B. F. Armaly, J. A. Drallmeier, Turbulent forced convection in a plane asymmetric diffuser: Effect of diffuser angle, J. Heat Trans.-T. ASME 131 (2009).

[13] M. J. Cervantes, T. F. Engström, Pulsating turbulent flow in a straight asymmetric diffuser, J. Hydraul. Res. 46(1) (2008) 112–128.

[14] R. D. Mehta, P. Bradshaw, Design rules for small low speed wind tunnels, Aeronaut. J. 83(827) (1979) 443–449.

[15] S. Obi, K. Aoki, S. Masuda, Experimental and computational study of turbulent separating flow in an asymmetric plane diffuser, In: Ninth symposium on turbulent shear flows, Kyoto, Japan 16-19 August 1993 (1993) 305.1–305.4.

[16] C. U. Buice, Experimental investigation of flow through an asymmetric plane diffuser, PhD. degree thesis, Department of Mechanical Engineering, Stanford University, available at me.stanford.edu/groups/thermo/pdf/TSD-107.pdf (1997).

[17] C. U. Buice, J. K. Eaton, Experimental investigation of flow through an asymmetric plane diffuser, J. Fluid Eng.-T. ASME 122(2) (2000) 433–435.

[18] H. J. Kaltenbach, M. Fatica, R. Mittal, T. S. Lund, P. Moin, Study of flow in a planar asymmetric diffuser using large-eddy simulation, J. Fluid Mech. 390 (1999) 151–185.

[19] X. Wu, J. Schlüter, P. Moin, H. Pitsch, G. Iaccarino, F. Ham, Computational study on the internal layer in a diffuser, J. Fluid Mech. 550 (2006) 391–412.

[20] A. Hellsten, P. Rautaheimo, In: Proceedings 8th ERCOFTAC IAHR/COST Workshop on Refined Turbulence Modelling, Helsinki, University of Technology (1999).

[21] D. D. Apsley, M. A. Leschziner, Advanced turbulence modelling of separated flow in a diffuser, Flow Turbul. Combust. 63 (1999) 81–112.

[22] G. Iaccarino, Predictions of a turbulent separated flow using commercial CFD codes, J. Fluid Eng.-T. ASME 123(4) (2001) 819–828.

[23] A. H. Herbst, P. Schlatter, D. S. Henningson, Simulations of turbulent flow in a plane asymmetric diffuser, Flow Turbul. Combust. 79 (2007) 275–306.

[24] S. M. El-Behery, M. Hamed, A comparative study of turbulence models performance for separating flow in a planar asymmetric diffuser, Comput. Fluids 44 (2011) 248–257.

[25] R. B. Dean, Reynolds number dependence of skin friction and other bulk flow variables in two-dimensional rectangular duct flow, J. Fluid Eng.-T. ASME 100 (1978) 215–223.

[26] ANSYS Fluent, Help system, Fluent 6.3 user's guide, ANSYS, Inc. (2006).

[27] D. C. Wilcox, Turbulence modeling for CFD, DCW Industries, Inc., La Cañada, California (1998).

[28] F. R. Menter, Two-equation eddy-viscosity turbulence models for engineering applications, AIAA J. 32(8) (1994) 1598–1605.

[29] B. E. Launder, D. P. Spalding, Mathematical models of turbulence, Imperial College of Science and Technology, Lectures Notes, London, England (1972).

[30] S. Poles, Y. Fu, E. Rigoni, The effect of initial population sampling on the convergence of multi-objective genetic algorithms, In: Multiobjective Programming and Goal Programming (Editors: V. Barichard, X. Gandibleux, V. T'Kindt), Springer Berlin Heidelberg (2009) 123–133.

[31] ModeFrontier, Modefrontier user's guide (version 4.0), www.esteco.com (2009).

[32] S. Poles, E. Rigoni, T. Robic, MOGA-II performance on noisy optimization problems, In: Proceedings of the International Conference on Bioinspired Optimization Methods and their Applications, Jozef Stefan Institute, Ljubljana (2004) 51–62.

[33] J. Serrin, Mathematical principles of classical fluid mechanics, In: Flügge S. (Ed.), Handbuch der Physik VIII/1, Springer-Verlag, Berlin (1959) 125–263.

[34] G. Buresti, Elements of Fluid Dynamics, Imperial College Press, London, 2012.

[35] S. Lim, H. Choi, Optimal shape design of a two-dimensional asymmetric diffuser in turbulent flow, AIAA J. 42(6) (2004) 1154–1169.

[36] B. S. Stratford, An experimental flow with zero skin friction throughout its region of pressure rise, J. Fluid Mech. 5 (1959) 17–35.

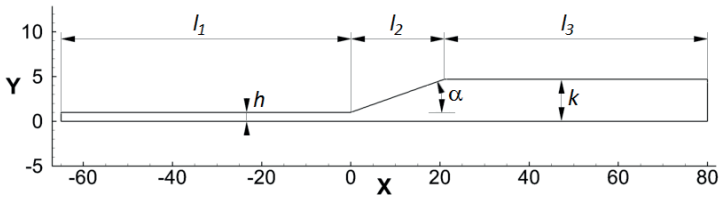

Figure 1: Diffuser geometry and reference frame

Grid	κ-ω	SST κ-ω	RSM
433×81	0.675	0.716	0.643
997×300	0.712	0.721	0.706
1994×600	0.725	0.727	0.714
3998×800	0.732	0.729	0.721

Table 1: $\overline{C_p}$ for the different turbulence models and the different computational grids

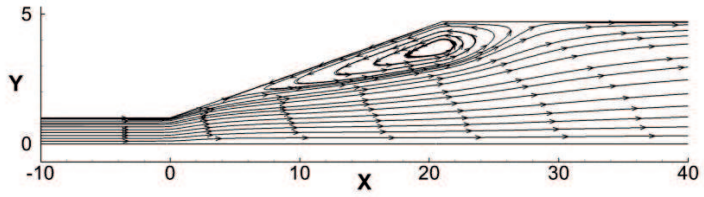

Figure 2: Streamlines inside the diffuser (SST κ-ω turbulence model)

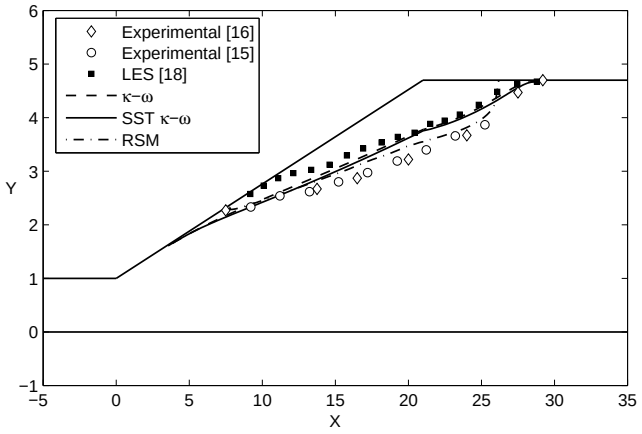

Figure 3: Positions where the streamwise velocity is equal to zero: comparison with the experimental data ([15, 16]) and numerical results ([18])

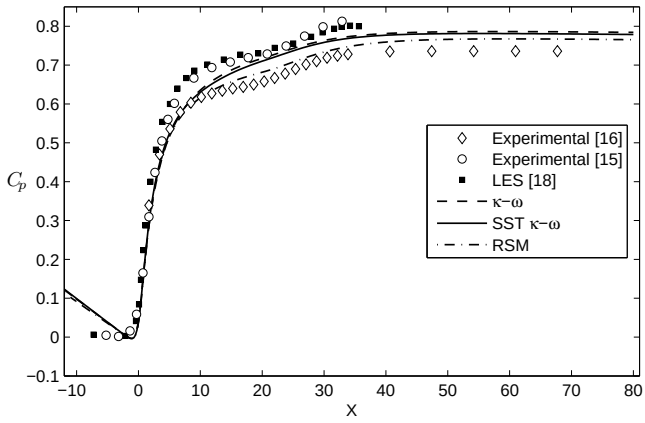

(a) Straight wall

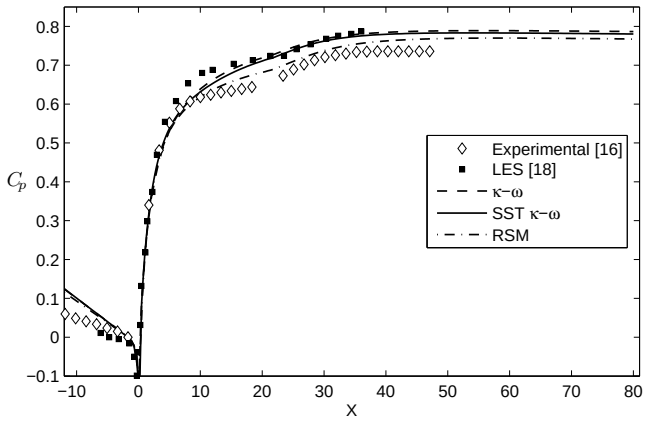

(b) Diverging wall

Figure 4: Pressure coefficient along the walls of the diffuser: comparison with the experimental data ([15, 16]) and numerical results ([18])

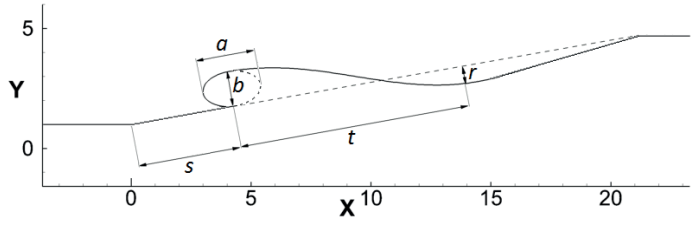

Figure 5: Geometry of the contoured cavity

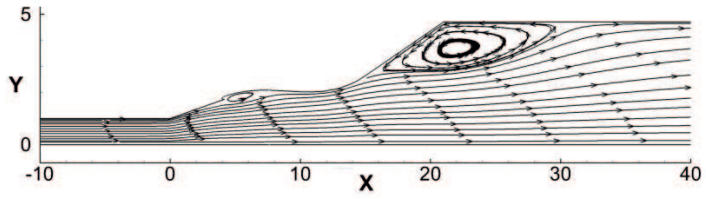

(a) Diffuser with optimized cavity

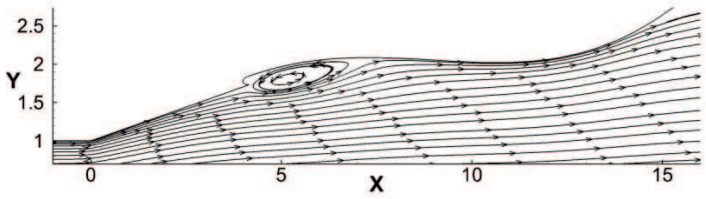

(b) Streamlines near to the optimized cavity

Figure 6: Streamlines in the diffuser with one optimized cavity

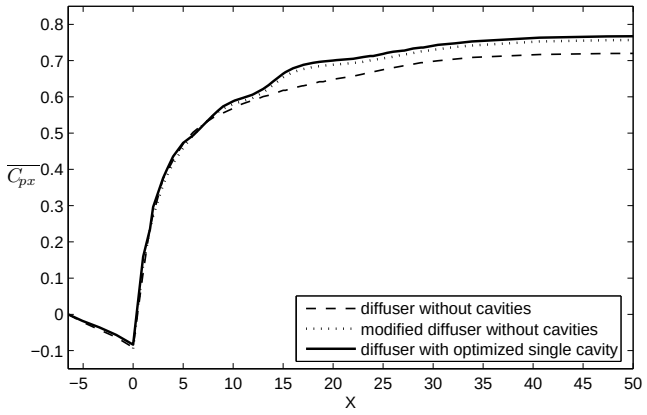

(a) Mean pressure coefficient at different X sections

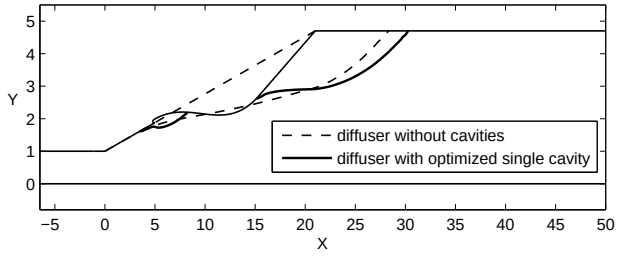

(b) Wall geometry and separated region extent

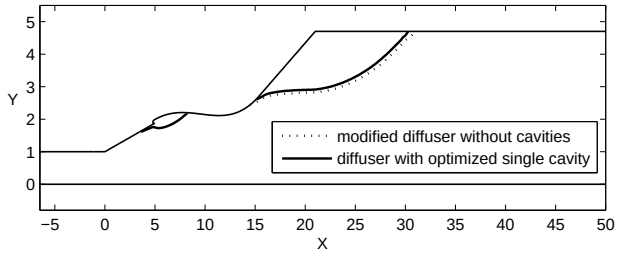

(c) Wall geometry and separated region extent

Figure 7: Mean pressure coefficient, wall geometry and separated region extent; comparison between the diffuser without cavities, the modified diffuser without cavities, and the diffuser with one optimized cavity

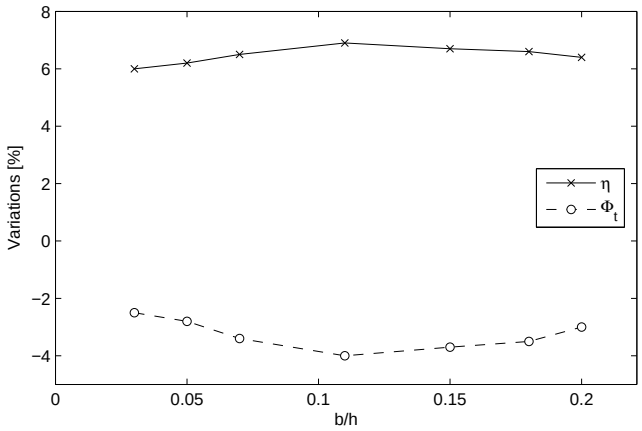

Figure 8: Effect of the variation of the parameter b/h

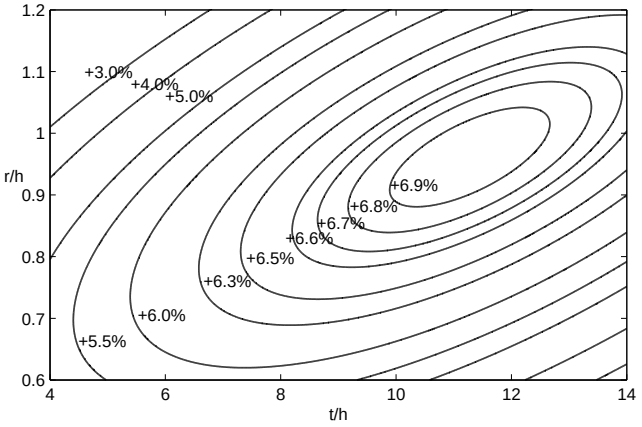

Figure 9: Effect of the variation of the parameters t/h and r/h on the diffuser efficiency

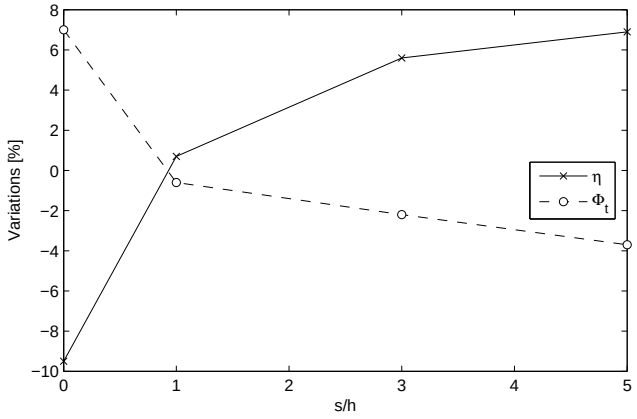

Figure 10: Effect of the variation of the parameter s/h

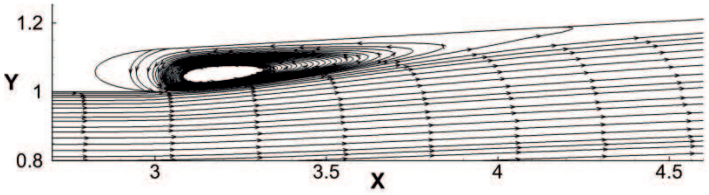

(a) Streamlines for the diffuser configuration analysed in [6]

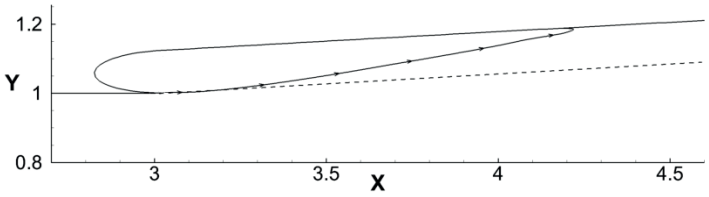

(b) Separated region extent and the wall of the reference diffuser (dashed line) for the diffuser configuration analysed in [6]

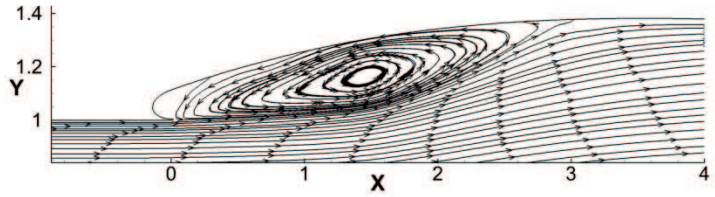

(c) Streamlines for the present diffuser configuration

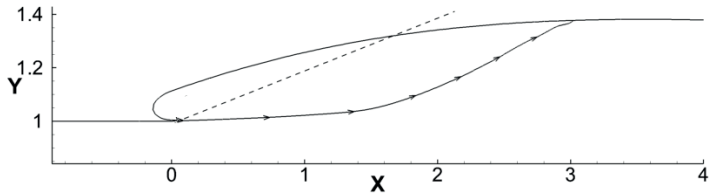

(d) Separated region extent and the wall of the reference diffuser (dashed line) for the present diffuser configuration

Figure 11: Comparison between the recirculation region in cavities located at the beginning of the diffuser diverging walls for the diffuser analysed in [6] and for the present one

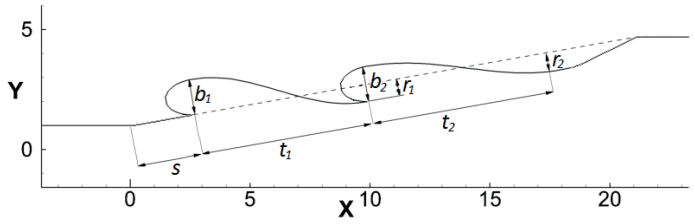

Figure 12: Geometry of two subsequent contoured cavities

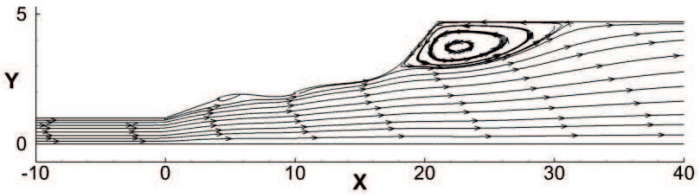

(a) Diffuser with optimized cavities

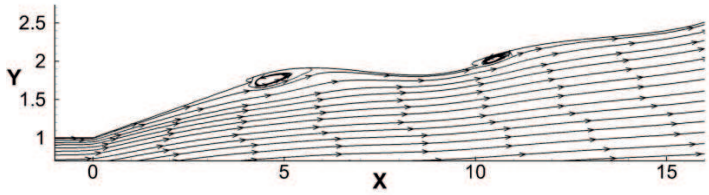

(b) Streamlines near to the optimized cavities

Figure 13: Streamlines in the diffuser with two subsequent optimized cavities

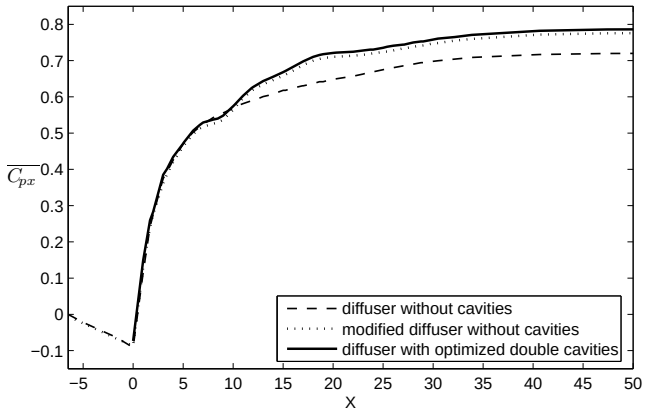

(a) Mean pressure coefficient at different X sections

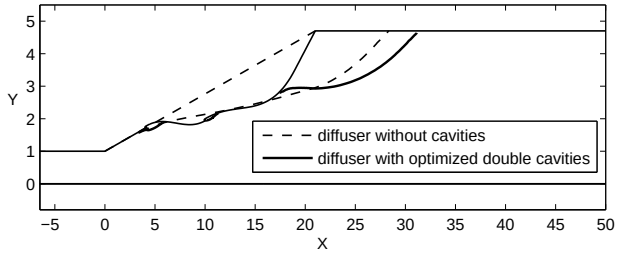

(b) Wall geometry and separated region extent

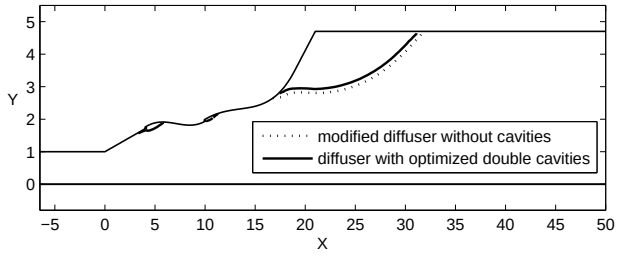

(c) Wall geometry and separated region extent

Figure 14: Mean pressure coefficient, wall geometry and separated region extent; comparison between the diffuser without cavities, the modified diffuser without cavities and the diffuser with two subsequent optimized cavities

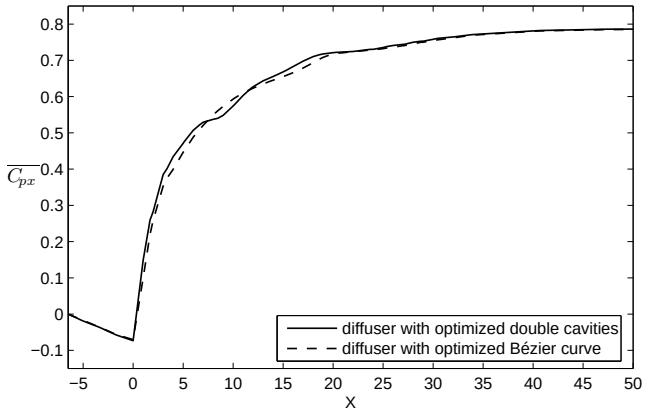

(a) Mean pressure coefficient at different X sections

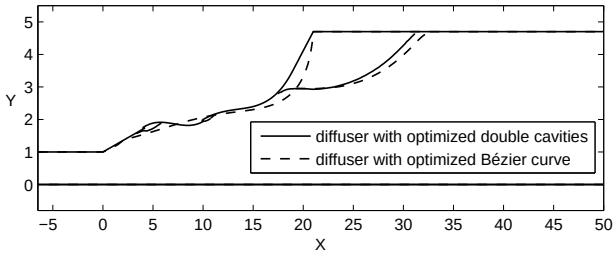

(b) Wall geometry and separated region extent

Figure 15: Mean pressure coefficient, wall geometry and separated region extent; comparison between the diffuser with two subsequent optimized cavities and the diffuser with optimized Bézier curves

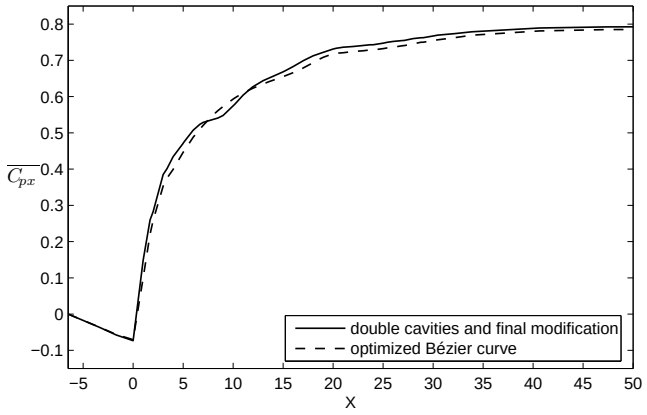

(a) Mean pressure coefficient at different X sections

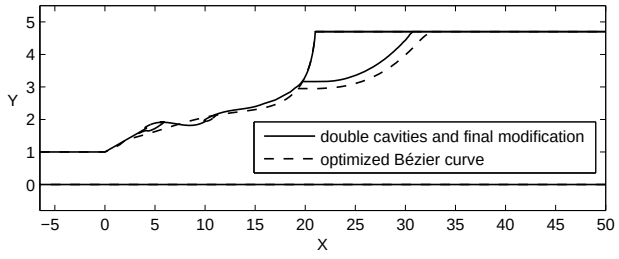

(b) Wall geometry and separated region extent

Figure 16: Mean pressure coefficient, wall geometry and separated region extent; comparison between the diffuser with two subsequent optimized cavities and final modification and the diffuser with optimized Bézier curves

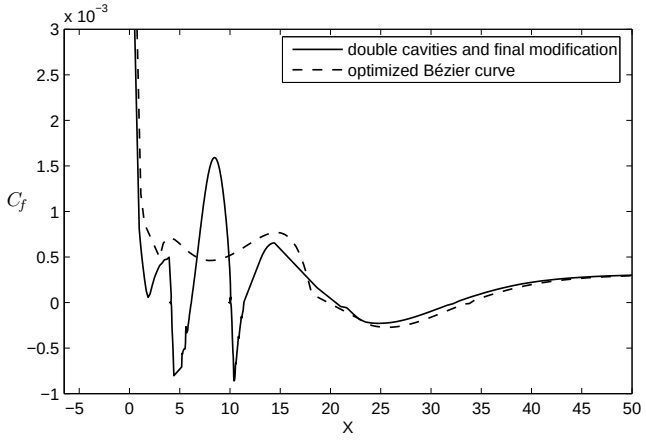

Figure 17: Skin friction coefficient along the diffuser diverging wall: comparison between the diffuser with two subsequent optimized cavities with final modification and the diffuser with optimized Bézier curves